Transportation Research Part C 155 (2023) 104317

Contents lists available at ScienceDirect

Transportation Research Part C

journal homepage: www.elsevier.com/locate/trc

Stability and extension of a car-following model for human-driven connected vehicles

Jie Sun [a], Zuduo Zheng [a,*], Anshuman Sharma [b,d], Jian Sun [c]

[a] School of Civil Engineering, The University of Queensland, St. Lucia 4072, Brisbane, Australia
[b] Department of Civil Engineering, Visvesvaraya National Institute of Technology, Nagpur 440010, India
[c] Department of Traffic Engineering & Key Laboratory of Road and Traffic Engineering, Ministry of Education, Tongji University, 4800 Cao'an Road, Shanghai 201804, China
[d] Department of Civil Engineering, Indian Institute of Technology (BHU), Varanasi 221005, India

ARTICLE INFO

Keywords:
Connected vehicle
Car-following
Human factors
Stability
Traffic oscillation
IDM

ABSTRACT

Despite the prosperous development of connected vehicle (*CV*) and its car-following (*CF*) models, human-driven *CV* and its *CF* properties are rarely investigated. This paper studies the stability characteristics of and then extends a recently-developed *CF* model of human-driven *CV* which incorporates human factors (*CV-CF* hereafter) by considering two levels of driver compliance, i.e., low compliance and high compliance. First, we investigate the stability of the *CV-CF* model, and validate the results with the simulation experiments. We then assess *CV*'s impact on the mixed traffic flow by deriving a stability criterion of heterogeneous traffic with the Laplace transform based method and analysing the influence of different levels of connectivity and their penetration rates. Furthermore, we extend the *CV-CF* model by considering two important additional human factors, i.e., time delay and estimation error, and evaluate different human factors' impact on the stability and oscillation characteristics of the *CV-CF* model. The results reveal that the connected environment indeed promotes the *CF* stability and alleviates traffic congestion, and that higher compliance to the information provided is generally more beneficial to the stability of traffic flow, except the situation with a large time delay.

1. Introduction

Connected vehicles (*CVs*), which are vehicles that can communicate with neighbouring vehicles (*V2V*) and infrastructure (*V2I*), are believed to have the potential to improve traffic flow with eased traffic congestion, better traffic safety, and lower traffic emissions (Diakaki et al., 2015). As one of the basic driving behaviours and the core of traffic flow theories, numerous efforts have been made on modelling the car-following (*CF*) behaviour of *CV* (Ge and Orosz, 2014; Jia and Ngoduy, 2016; Jia et al., 2019; Milanés and Shladover, 2014; Monteil et al., 2014; Talebpour et al., 2016; van Arem et al., 2006). However, a major limitation of previous studies is the ignorance or inadequate consideration of human factors, such as driver compliance. In addition, due to the lack of real-world *CV* trajectory data, these models cannot be realistically calibrated since they are developed on the basis of numerical experiments or trajectories of traditional human-driven vehicles with some strong assumptions. Therefore, Sharma et al. (2019a) proposed a connected vehicle *CF* model (*CV-CF*) by incorporating the driver compliance behaviour (one of the critical human factors for the success of

* Corresponding author.
E-mail address: zuduo.zheng@uq.edu.au (Z. Zheng).

https://doi.org/10.1016/j.trc.2023.104317
Received 9 July 2022; Received in revised form 21 August 2023; Accepted 22 August 2023
Available online 4 September 2023

this technology) that can be integrated with classical *CF* models to realistically describe the longitudinal vehicular movements of *CV*. They validated the soundness of the *CV-CF* model with *CV* trajectory data collected from well-designed driving simulator experiments. Particularly, two levels of driver compliance (i.e., high compliance and low compliance) were described based on the Prospect Theory (Kahneman and Tversky, 2013), as it can capture both rational and irrational decision-making mechanisms of drivers. Thanks to its capability of realistically capturing *CV* behaviour, the *CV-CF* model has been used in Jia et al. (2021); Rahman et al. (2021); Sharma et al. (2021) for the investigation of traffic flow characteristics in a connected environment.

However, for this *CV-CF* model, its string stability properties remain unexplored. As the internal rationale of traffic oscillation - a commonly observed phenomenon in congested traffic (Chandler et al., 1958; Orosz et al., 2010; Wilson and Ward, 2011), the string stability of *CF* behaviour is one of the fundamental characteristics of *CF* models, which describes how a small perturbation evolves over a platoon. The stability analysis of *CF* models has been prevailing for more than 60 years since the early days of *CF* modelling (Bando et al., 1998; Chandler et al., 1958; Herman et al., 1959; Monteil et al., 2014; Ngoduy, 2015; Orosz et al., 2011; Orosz et al., 2009; Sau et al., 2014; Sau et al., 2019; Sun et al., 2018, 2020, 2023; Swaroop and Hedrick, 1996; Treiber and Kesting, 2013; Zhang and Jarrett, 1997) and used to facilitate the development of *CV-CF* model (Zhang and Orosz, 2016; Zhou et al., 2020). As there is no consistent conclusion of the impact of connected environment on the traffic flow's stability and because of the scarcity of realistic *CV-CF* model in the literature (especially for human-driven *CV*), one main purpose of this paper is to assess the string stability of the *CV-CF* model proposed in Sharma et al. (2019a) both theoretically and numerically. Considering the multi-level of driver compliance and future mixed traffic flow, we scrutinise the stability criterion of heterogeneous traffic with the Laplace transform based method, and analyse the impact of different levels of connectivity and their penetration rates on the mixed traffic flow.

The conventional studies on stability analysis have been based on the strict assumption of homogeneous traffic, which impedes its applicability given the fact that *CVs* will coexist with traditional human-driven vehicles in the foreseeable future leading to a mixed traffic flow (Sun et al., 2018). To apply the stability analysis on mixed traffic flow, Ward (2009) and Ngoduy (2013) successively derived a stability criterion of heterogenous traffic using the characteristic equation based method (i.e., based on the characteristic equation induced from linearised *CF* models with the use of exponential ansatz to represent perturbations). This stability criterion has been broadly adopted in studies on the characteristics of mixed traffic flow (Talebpour and Mahmassani, 2016; Xie et al., 2018) bringing more insight for the understanding of connected environment. Recently, Montanino and Punzo (2021) revisited this stability criterion and pointed out its limitation in finite-length platoon. In addition, as per Sun et al. (2018), the stability criterion derived from different methods may be inconsistent with each other. In this context, we attempt to examine the theoretical stability analysis of heterogenous traffic with Laplace transform based method in this study and measure the impact of *CV-CF* model with different compliance levels on the mixed traffic flow.

Furthermore, human factors are critical in revealing the *CF* behaviour and explaining many complex traffic phenomena, such as vehicle crash and traffic oscillation, in both the traditional and connected environments (Sharma et al., 2017; van Lint and Calvert, 2018). The connected technology can alter driver behaviours, positively or negatively. Although driver compliance to information has been incorporated in the *CV-CF* model, some other common human factors such as time delay, estimation error and driver capability were omitted for simplicity, despite that these human factors also play an important role in the human-driven *CV*. Therefore, another motivation of this study is to extend the *CV-CF* model by considering additional human factors and testify their impact on traffic stability and oscillation based on the extended *CV-CF* model. More specifically, we respectively incorporate the time delay and estimation error into the model and probe the effect of different human factors on the stability and oscillation characteristics of the *CV-CF* model. In summary, the main contributions of this paper are as below:

- We have investigated the stability properties of a newly proposed *CF* model for connected vehicles both theoretically and numerically, which is a challenging task due to the complicated mathematical forms and different levels of compliance considered in this new *CV-CF* model;
- We have derived the stability criterion of heterogenous traffic with the Laplace transform based method, and analysed the impact of different levels of connectivity (communication delay or loss) and their penetration rates on the mixed traffic flow;
- We have extended the *CV-CF* by considering time delay and estimation error and investigated the new models' stability and oscillation features.

The remainder of this paper is organised as follows: in Section 2 we introduce the *CV-CF* model with driver compliance and study its stability; in Section 3 we develop the theoretical stability criterion for the mixed traffic; in Section 4 and Section 5, we explore the impact of time delay and estimation error on the *CV-CF* model's stability, respectively; and finally in Section 6 we summarise and discuss the main findings of this study.

2. Stability analysis of *CV-CF* model

Driver compliance is a key human factor that should be considered in the connected environment. As stated before, although the modelling of *CV*'s *CF* behaviour has been widely studied, most of the *CF* models for *CVs* assume that the driver fully complies with the provided information, which is not realistic in real world. We thus first introduce the *CV-CF* model that incorporates the driver compliance in Sharma et al. (2019a) and then study its stability in this section.

2.1. CV-CF model with driver compliance

In the *CV-CF* model, it is assumed that a driver's compliance depends on the observed time gap[1] (spacing divided by speed, excluding vehicle length) at the time of information display (Sharma et al., 2019a). As time gap decreases, drivers comply more and vice versa. Thus, the usefulness of the provided information increases with the time gap decreases. The compliance of a driver in response to the information is categorised as low compliance, or high compliance levels. Different compliance levels mean that drivers weight provided information differently within a subjective headway range, as high compliance weights more with smaller time gap and low compliance wights more with larger time gap. The complete compliance level utility is thus defined based on the Prospect Theory as a product of usefulness and weight (*Complianceutility* $=$ *usefulness* $\times$ *weight*). (In terms of using the Prospect Theory to model traditional CF behaviours, please refer to nice papers by Prof Hamdar and his colleagues (Hamdar et al., 2020; Hamdar et al., 2008; Talebpour et al., 2011).).

The usefulness denotes how useful an information is to a driver, whereas the weight denotes how much a driver weighs the information at different compliance levels. The usefulness value associated with the observed time gap is $V(h_{obs})$ and is calculated using usefulness value function which describes the inverse proportionality between the observed time gap and the usefulness value as shown in Eq. (1).

$$V(h_{obs}) = \frac{1}{(1 + e^{\lambda(\alpha h_{obs} - 1)})} \tag{1}$$

where λ and α are the parameters that govern the shape of the function, and h_{obs} is the observed time gap at a given time.

Similar to the probability weighting element of the Prospect Theory, it is hypothesised that a driver overweighs the warning information when the time gap is small (due to high risk) and underweights it when the time gap is large. The magnitude of the weight at a particular compliance level is governed by the probability of the observed time gap falling in the time gap range of that level. The probabilities that an observed time gap will fall under low and high compliance time gap ranges are represented by P_{LC} and P_{HC}, respectively, and the corresponding weights are $W^{LC}(P_{LC})$ and $W^{HC}(P_{HC})$ which are calculated using weighting functions same as Prospect Theory weighting function. The weighting functions and the probability that an observed time gap falls in a driver's compliance range are given by Eqs. (2)–(5), respectively.

$$W^{LC}(P_{LC}) = \frac{{P_{LC}}^{\gamma}}{({P_{LC}}^{\gamma} + (1 - P_{LC})^{\gamma})^{1/\gamma}} \tag{2}$$

$$P_{LC} = \min\left(\frac{h_{obs}}{h_{max}}, 1\right) \tag{3}$$

$$W^{HC}(P_{HC}) = \frac{{P_{HC}}^{\gamma}}{({P_{HC}}^{\gamma} + (1 - P_{HC})^{\gamma})^{1/\gamma}} \tag{4}$$

$$P_{HC} = \min\left(\frac{h_{min}}{h_{obs}}, 1\right) \tag{5}$$

where γ is the shape parameter. As h_{obs} increases and approaches to h_{max}, the low compliance weight increases and approaches to 1, while as h_{obs} decreases and approaches to h_{min}, the high compliance weight increases and approaches to 1.

Therefore, the compliance utilities of low and high compliance levels are obtained as below:

$$U(h_{obs}, i) = V(h_{obs}) W^{i}(P_i) \tag{6}$$

where i represent the compliance level and is equal to *LC* for the low compliance, and *HC* for the high compliance. The maximum utility is denoted by U that ranges from 0 to 1, with $U = 0$ representing no compliance and $U = 1$ representing the full compliance.

The compliance with information leads to change in *CF* behaviour in the connected environment. A comparison of microscopic traffic flow parameters (e.g., average headway, average spacing, average speed, fluctuations in speed and spacing) between the traditional and connected scenarios from the driving simulator experiments revealed that, vehicles' headway increases and acceleration behaviour becomes more stable in the connected scenario. As the time gap and headway are directly proportional to each other, thus, the time gap parameter in *CF* models is multiplied with $1 + U(h_{obs})$ to accommodate the impact of driver compliance with continuous information (Sharma et al., 2019a). It should be noted that this *CV-CF* model do not consider drivers who might maintain a lower time gap in the connected environment which is a limitation of the model. This heterogeneity in the time gap maintaining behaviour will be incorporated in future studies.

For the purpose of illustration, and while other *CF* models can be applied by following the same process, intelligent driver model (*IDM,* Treiber et al., 2000) is selected to integrated with compliance utility function as *CV-IDM*, due to two main reasons: (i) *IDM* is

[1] Note that in the original paper, observed time headway is used since the information/warnings were provided/triggered based on space headway rather than space gap. To be more realistic and consistent with the basic CF model in this study, i.e., IDM, where the observed space gap and desired time gap are used, we modify the observed time headway with observed time gap.

widely used in the literature, and is capable of satisfactorily reproducing many characteristics of traffic flow, in particular, the stop-and-go oscillation characteristic; and (ii) the model's stability is also analysed in the literature (Ngoduy, 2013; Ngoduy, 2015; Sun and Sun, 2018; Sun et al., 2018, 2020; Treiber and Kesting, 2013).

$$a_n(s_n, v_n, \Delta v_n) = a\left[1 - \left(\frac{v_n}{v_0}\right)^{\delta} - \left(\frac{s^*}{s_n}\right)^2\right] \tag{7}$$

$$s^* = s_0 + (1 + U(h_{obs}, i))Tv_n - \frac{v_n \Delta v_n}{2\sqrt{ab}} \tag{8}$$

where v_0 is the desired speed; $s_n^*(t)$ is the desired gap; s_0 is the minimum gap in the standstill situation; T is the desired time gap; a is the maximum acceleration; b is the comfortable deceleration; and δ is free acceleration exponent. The default parameters of the *CV-CF* model are presented in Table 1 unless stated otherwise.

It is noted that Sharma et al. (2019a) proposed a connected vehicle driving strategy that describes driver's behaviour in response to a continuous information and advanced event triggered information, and consequently has two components. This study focuses only on the continuous information component for mainly three reasons: 1) the event-triggered information is provided only in a specific scenario-leader braking hard, while the continuous information is provided all the time. The *CV-CF* model works with the continuous information component most time without the influence of event-triggered information, as the majority of existing models for connected and/or automated vehicles do. 2) As the linear string stability focuses on the stability characteristics of a system under the influence of a small perturbation, it requires that the platoon is only experiencing small disturbances (e.g., 1 m/s^2 deceleration for 3 s) which naturally does not involve the event-triggered information. 3) the simplified *CV-CF* model has been used in several recent studies, e.g., Jia et al. (2021); Rahman et al. (2021); Sharma et al. (2021) for the investigation of traffic flow characteristics in a connected environment, and the soundness of this simplification has been clearly demonstrated. For more details of the original CV-CF model, please refer to Sharma et al. (2019a).

With two classes of driver compliance for *CV*, low compliance-*IDM* (*LC-IDM*) and high compliance-*IDM* (*LC-IDM*) could be developed separately, by deploying different compliance utility functions. The stability of the two models will be analysed in detail in the next subsection.

2.2. Stability of CV-CF models

According to the literature (Sun et al., 2018; Treiber and Kesting, 2013; Wilson, 2008; Wilson and Ward, 2011), there is a general string stability criterion for basic *CF* models (without considering any time delays), as shown in Eq. (9):

$$\frac{1}{2} - \frac{f_{\Delta v}}{f_v} - \frac{f_s}{f_v^2} > 0 \tag{9}$$

where $f_s = \frac{\partial f}{\partial s}|_e, f_v = \frac{\partial f}{\partial v}|_e, f_{\Delta v} = \frac{\partial f}{\partial \Delta v}|_e$ are the Taylor expansion coefficients of the acceleration function at the steady state in terms of different variables after the first-order linearisation.

CV-IDM's stability criterion can be constructed by using its Taylor expansion coefficients, as shown in Eqs. (10)–(12) according to this string stability criterion.

$$f_s = -2a\left(\frac{s_0 + (1 + UT(h_e))Tv_e}{s_e}\right)\frac{(s^*)_s' s_e - (s_0 + (1 + UT(h_e))Tv_e)}{s_e^2} \tag{10}$$

$$f_v = -a\left[\frac{\delta}{v_0}\left(\frac{v_e}{v_0}\right)^{\delta-1} + \frac{2(s_0 + (1 + UT(h_e))Tv_e)(s^*)_v'}{s_e^2}\right] \tag{11}$$

$$f_{\Delta v} = \sqrt{\frac{a}{b}}\frac{v_e}{s_e}\frac{s_0 + (1 + UT(h_e))Tv_e}{s_e} \tag{12}$$

where v_e and s_e denote the equilibrium speed and the equilibrium spacing in homogenous traffic, respectively, and h_e denotes the equilibrium time gap $h_e = \frac{s_e}{v_e}$; $(s^*)_s', (s^*)_v'$ are distinct for *LC-IDM* and *HC-IDM* models as shown in Eqs. (13)–(14) and Eqs. (15)–(16),

Table 1
Default parameters of the *CV-CF* model.

Desired speed v_0	120 km/h	lambda λ	6
Desired time gap T	1 s	alpha α	0.2 s^{-1}
Minimum gap s_0	2 m	gamma γ	0.65
Acceleration a	1 m/s^2	Minimum time gap h_{min}	1 s
Comfortable deceleration b	1.5 m/s^2	Maximum time gap h_{max}	10 s
Acceleration exponent δ	4		
Vehicle length l	5 m		

respectively, since the time gap probabilities are different for them. For conditions that $h_{obs} > h_{max}$ for *LC-IDM* and $h_{obs} < h_{min}$ for *HC-IDM*, we can simplify the stability criteria Eqs. (10)–(16) with $P_e = 1$, which is not presented here for the purpose of concise.

$$(s^*)'_{s,LC} = Tv_e \left(\begin{array}{c} \frac{-e^{\lambda(ah_e-1)}\lambda\alpha}{\left(1+e^{\lambda(ah_e-1)}\right)^2 v_e} \frac{{P_e}^{\gamma}}{\left({P_e}^{\gamma}+(1-P_e)^{\gamma}\right)^{1/\gamma}} + \frac{1}{\left(1+e^{\lambda(ah_e-1)}\right)} \frac{1}{h_{max}v_e} \times \\ \frac{\gamma {P_e}^{\gamma-1}\left(\left({P_e}^{\gamma}+(1-P_e)^{\gamma}\right)^{1/\gamma}\right) - 1/\gamma {P_e}^{\gamma}\left({P_e}^{\gamma}+(1-P_e)^{\gamma}\right)^{1/\gamma-1}\left(\gamma {P_e}^{\gamma-1}-\gamma(1-P_e)^{\gamma-1}\right)}{\left({P_e}^{\gamma}+(1-P_e)^{\gamma}\right)^{2/\gamma}} \end{array} \right) \tag{13}$$

$$(s^*)'_{v,LC} = (1+UT(h_e))T + Tv_e \left(\begin{array}{c} \frac{e^{\lambda(ah_e-1)}\lambda\alpha s_e}{\left(1+e^{\lambda(ah_e-1)}\right)^2 v_e^2} \frac{{P_e}^{\gamma}}{\left({P_e}^{\gamma}+(1-P_e)^{\gamma}\right)^{1/\gamma}} - \frac{1}{\left(1+e^{\lambda(ah_e-1)}\right)} \frac{s_e}{h_{max}v_e^2} \times \\ \frac{\gamma {P_e}^{\gamma-1}\left(\left({P_e}^{\gamma}+(1-P_e)^{\gamma}\right)^{1/\gamma}\right) - 1/\gamma {P_e}^{\gamma}\left({P_e}^{\gamma}+(1-P_e)^{\gamma}\right)^{1/\gamma-1}\left(\gamma {P_e}^{\gamma-1}-\gamma(1-P_e)^{\gamma-1}\right)}{\left({P_e}^{\gamma}+(1-P_e)^{\gamma}\right)^{2/\gamma}} \end{array} \right) \tag{14}$$

$$(s^*)'_{s,HC} = Tv_e \left(\begin{array}{c} \frac{-e^{\lambda(ah_e-1)}\lambda\alpha}{\left(1+e^{\lambda(ah_e-1)}\right)^2 v_e} \frac{{P_e}^{\gamma}}{\left({P_e}^{\gamma}+(1-P_e)^{\gamma}\right)^{1/\gamma}} - \frac{1}{\left(1+e^{\lambda(ah_e-1)}\right)} \frac{h_{min}v_e}{s_e^2} \times \\ \frac{\gamma {P_e}^{\gamma-1}\left(\left({P_e}^{\gamma}+(1-P_e)^{\gamma}\right)^{1/\gamma}\right) - 1/\gamma {P_e}^{\gamma}\left({P_e}^{\gamma}+(1-P_e)^{\gamma}\right)^{1/\gamma-1}\left(\gamma {P_e}^{\gamma-1}-\gamma(1-P_e)^{\gamma-1}\right)}{\left({P_e}^{\gamma}+(1-P_e)^{\gamma}\right)^{2/\gamma}} \end{array} \right) \tag{15}$$

$$(s^*)'_{v,HC} = (1+UT(h_e))T + Tv_e \left(\begin{array}{c} \frac{e^{\lambda(ah_e-1)}\lambda\alpha s_e}{\left(1+e^{\lambda(ah_e-1)}\right)^2 v_e^2} \frac{{P_e}^{\gamma}}{\left({P_e}^{\gamma}+(1-P_e)^{\gamma}\right)^{1/\gamma}} + \frac{1}{\left(1+e^{\lambda(ah_e-1)}\right)} \frac{h_{min}}{s_e} \times \\ \frac{\gamma {P_e}^{\gamma-1}\left(\left({P_e}^{\gamma}+(1-P_e)^{\gamma}\right)^{1/\gamma}\right) - 1/\gamma {P_e}^{\gamma}\left({P_e}^{\gamma}+(1-P_e)^{\gamma}\right)^{1/\gamma-1}\left(\gamma {P_e}^{\gamma-1}-\gamma(1-P_e)^{\gamma-1}\right)}{\left({P_e}^{\gamma}+(1-P_e)^{\gamma}\right)^{2/\gamma}} \end{array} \right) \tag{16}$$

2.3. Stability analysis results

To compare the stability between *IDM* and *CV-IDM*, we plot the stability regions to illustrate the stability conditions for different models by varying desired time gap T and maximum acceleration a while fixing other parameters as per Sun et al. (2018). It is worth noting that solving the equation of the equilibrium spacing and speed with respect to time gap for *CV-IDM* is non-trivial and can be only done numerically, we calculate the stability of 1600 combinations of desired time gap (0.1–4 s) and maximum acceleration (0.1–4 m/s^2) for *LC-IDM* and *HC-IDM*, while other parameters are default.

As we can see from Fig. 1, the stability is improved for both *LC-IDM* and *HC-IDM* compared to *IDM*, while *HC-IDM* is much more stable than *LC-IDM*, especially when desired time gap is between 0.5 and 2 s, a range that covers the majority of human-drivers. Meanwhile, the improvement of its stability is negligible for *LC-IDM* when desired time gap is smaller than 2 s. Such finding reveals the important role of driver compliance to the information in the connected environment: a higher compliance of drivers to the

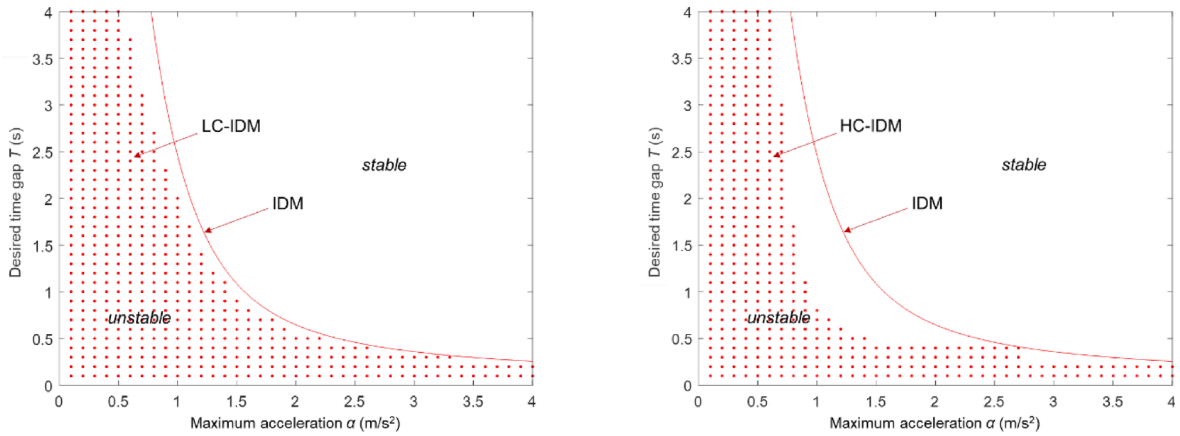

(a) *LC-IDM* (b) *HC-IDM*

Fig. 1. Theoretical stability regions for *CV-IDMs* (The solid line denotes the boundary of the theoretical criterion for *IDM*; the points denote the theoretical string unstable parameter sets for *CV-IDMs*.).

received information brings a higher stability.

To validate the theoretical results of *CV-IDMs*, we conduct numerical simulations of the two models by introducing a small disturbance to a platoon of vehicles to see how the disturbance evolves over vehicles (if the disturbances strictly decrease along the platoon, the platoon is string stable; otherwise, it is string unstable). Following the setup in Sun et al. (2018), a platoon of identical vehicles enters a very long, single-lane straight road and quickly reach the equilibrium state, driving at the same speed (10 m/s or 36 km/h) with the corresponding equilibrium gap. At $t = 60$ s, a disturbance is introduced to the first leading vehicle by forcing it to first decelerate and then accelerate for the same time duration (for the sake of simplicity, in this study, the first vehicle decelerated with 1 m/s^2 for 3 s and then accelerated with 1 m/s^2 for 3 s, thus the magnitude of the disturbance is 3 m/s). After experiencing the disturbance, vehicles converge to the original equilibrium state.

In each simulation step, the following vehicles move forward according to the *CV-IDMs*, while the speed and position of vehicles are updated with the trapezoidal rule, as shown in Eqs. (17) and (18) (Treiber and Kanagaraj, 2015). The speeds of vehicles are collected for analysing the platoon's stability, as the disturbance is denoted as the absolute speed deviation from the equilibrium speed.

$$v_n(t+\Delta T) = v_n(t) + \frac{1}{2}\left(a_n(t) + a_n(t+\Delta T)\right)\Delta T \tag{17}$$

$$x_n(t+\Delta T) = x_n(t) + v_n(t)\Delta T + \frac{a_n(t)(\Delta T)^2}{2} \tag{18}$$

Based on the results for all the simulation runs, we plot the stability regions of *HC-IDM* and *LC-IDM* as shown in Fig. 2. The dots represent the string unstable parameter sets from simulation for *CV-IDMs*. Compared to the theoretical results as shown in Fig. 1, we know that the simulation results are highly consistent with the theoretical results, which accords with the result in Sun et al. (2018) that the consistency between theoretical results and simulation results for models without time delay is very high (above 98%).

Notably, although the *CV-CF* models can largely improve the stability, the results induced from the equilibrium flow show that the theoretical maximum capacity will be reduced, which is one potential limitation of the model. However, as the experiments from Sharma et al. (2021) suggest that in a realistic traffic oscillation scenario, the *CV-CF* models will enhance the traffic efficiency in a mixed traffic flow of both traditional and connected human-driven vehicles. This implies that better stability is beneficial for the traffic efficiency in congested flow. Nevertheless, readers should also have a careful look at the traffic efficiency impact when applying the *CV-CF* models, especially in equilibrium flow. More in-depth investigations for the relationship between stability and efficiency is needed in future research. For example, some simple yet efficient control strategies, such as improving the responsiveness of vehicles by increasing the maximum acceleration parameter of IDM, can be applied to improve both the stability and efficiency of traffic flow.

3. Stability analysis of mixed traffic flow

Given that different compliance levels of *CVs* will coexist with traditional human-driven vehicles in the near future, it is critical to analyse the stability of the mixed traffic flow. Despite that a stability criterion of heterogenous traffic using the characteristic equation based method has been proposed by Ward (2009) and Ngoduy (2013), considering the potential discrepancy between stability criterions derived from different methods, in this section, we revisit the theoretical stability analysis of heterogenous traffic using the Laplace transform based method and evaluate the influence of *CV*'s compliance level on the mixed traffic flow.

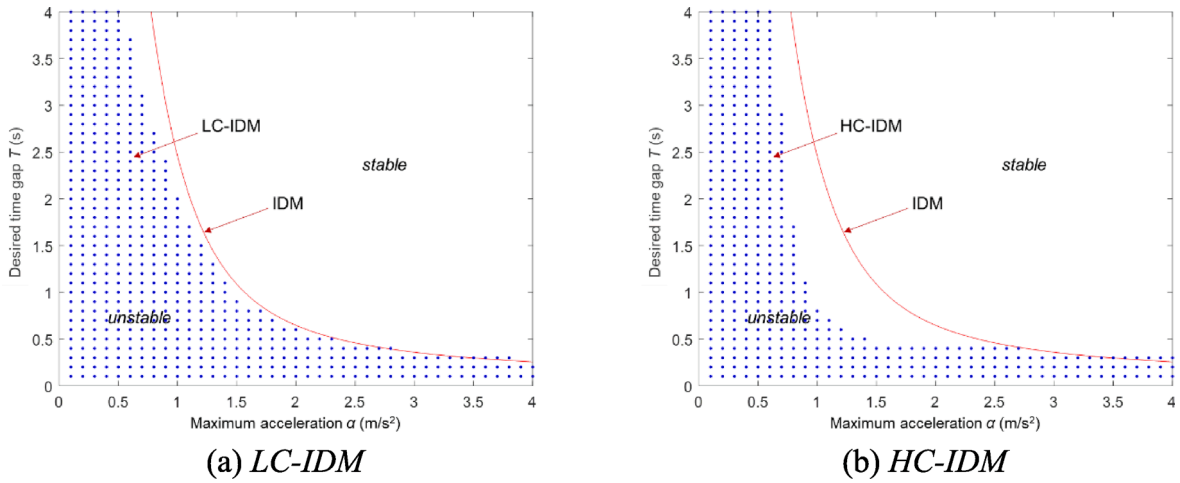

(a) *LC-IDM* (b) *HC-IDM*

Fig. 2. Stability regions from simulation for *CV-IDMs* (The solid line denotes the boundary of the theoretical criterion for *IDM*; the points denote the string unstable parameter sets from simulation for *CV-IDMs*; the magnitude of the disturbance in this scenario is 3 m/s: the first vehicle decelerated with 1 m/s^2 for 3 s and then accelerated with 1 m/s^2 for 3 s.).

3.1. Laplace transform based method for mixed traffic flow

As per Sun et al. (2018); Treiber and Kesting (2013), to be string stable the perturbation (i.e. the spacing/speed deviation from the equilibrium spacing/speed that is used as the indicator) needs to strictly attenuate for each leader–follower pair as it propagates along a platoon where vehicle n follows vehicle (n-1), as formulated in Eq. (19):

$$\|\varepsilon_1\|_\infty > \|\varepsilon_2\|_\infty > \cdots > \|\varepsilon_k\|_\infty > \cdots > \|\varepsilon_n\|_\infty \tag{19}$$

where $\|\varepsilon_k\|_\infty = max_t|\varepsilon_k|$ is the maximum magnitude of the kth vehicle's perturbation within infinite time. It is unstable if any leader–follower pair in the platoon is not satisfied.

To obtain the stability criterion, Laplace transform can facilitate the string stability analysis of a system by transforming the system from the time domain to the frequency domain (Orosz et al., 2011; Orosz et al., 2010; Sun et al., 2018). The relationship of the perturbation between two consecutive vehicles in the frequency domain is:

$$G(s) = \frac{E_n(s)}{E_{n-1}(s)} = \frac{sf_{\Delta v} + f_s}{s^2 - s(f_v - f_{\Delta v}) + f_s} \tag{20}$$

where $E_n(s)$ is the Laplace transform of $\varepsilon_n(t)$.

We assume a mixed platoon consisted of n types of vehicles (a total of N vehicles) governed by different *CF* models with probabilities of $p_1, \cdots, p_k, \cdots, p_n$, with each type contains $p_1N, \cdots, p_kN, \cdots, p_nN$ vehicles (without the loss of generality, we assume p_kN is an integer). A platoon is considered as being stable when the perturbations are attenuated when they propagate from the head to the tail (the evolution of perturbations within the platoon is ignored), which is also known as weak string stability (Ge and Orosz, 2014; Montanino and Punzo, 2021). The head to tail transfer function of perturbations in the frequency domain is:

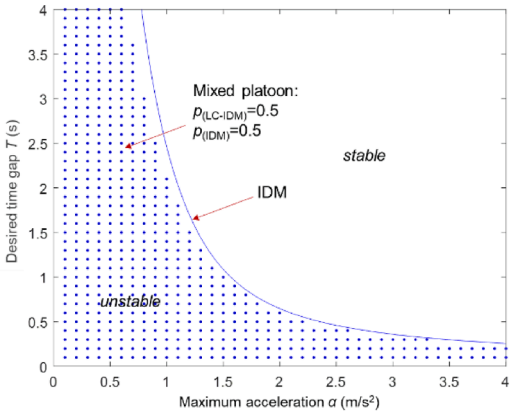

(a) *LC-IDM* and *IDM*; $p_{(LC\text{-}IDM)} = p_{(IDM)} = 0.5$

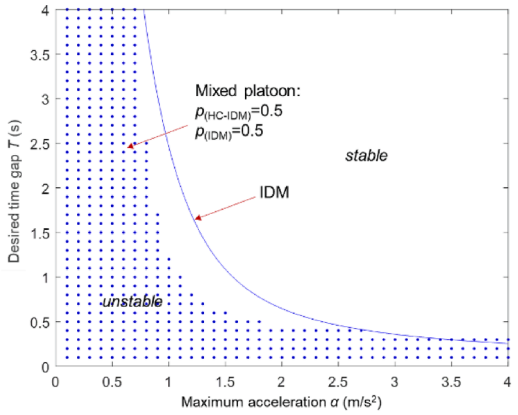

(b) *HC-IDM* and *IDM*; $p_{(HC\text{-}IDM)} = p_{(IDM)} = 0.5$

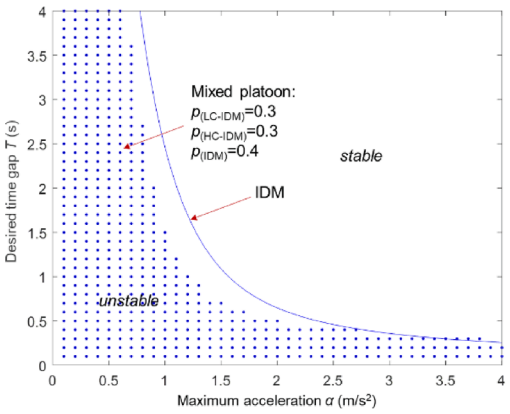

(c) *LC-IDM*, *HC-IDM* and *IDM*; $p_{(LC\text{-}IDM)} = p_{(HC\text{-}IDM)} = 0.3$, $p_{(IDM)} = 0.4$

Fig. 3. Theoretical stability regions for mixed platoon (the solid line denotes the boundary of the theoretical criterion for *IDM*; the points denote the theoretical string unstable parameter sets for mixed platoon.).

$$G(s)=\frac{E_n(s)}{E_1(s)}=\prod_{i=1}^{N}G_i(s)=G_1(s)^{p_1N}\cdots G_k(s)^{p_kN}\cdots G_n(s)^{p_nN} \tag{21}$$

The necessary and sufficient condition for the head-to-tail string stability is given by $|G(i\omega)|\langle 1$, and by setting $s=i\omega$ to initialise a steady signal in the frequency domain, we have:

$$|G(i\omega)|=\prod_{k=1}^{n}\left|\frac{i\omega f_{\Delta v}^{k}+f_s^k}{-\omega^2-i\omega(f_v^k-f_{\Delta v}^k)+f_s^k}\right|^{p_kN}=\prod_{k=1}^{n}\left(\frac{\sqrt{\omega^2\left(f_{\Delta v}^k\right)^2+\left(f_s^k\right)^2}}{\sqrt{\left(f_s^k-\omega^2\right)^2+\omega^2\left(f_v^k-f_{\Delta v}^k\right)^2}}\right)^{p_kN}<1 \tag{22}$$

Given $|G(i\omega)|\rangle 0$, by taking the natural logarithm of both sides, the condition becomes:

$$\begin{aligned}\ln|G(i\omega)|&=\sum_{k=1}^{n}\frac{p_kN}{2}\ln\frac{\omega^2\left(f_{\Delta v}^k\right)^2+\left(f_s^k\right)^2}{\left(f_s^k-\omega^2\right)^2+\omega^2\left(f_v^k-f_{\Delta v}^k\right)^2}=\sum_{k=1}^{n}\frac{p_kN}{2}\ln\left(1+\frac{\omega^2\left(f_{\Delta v}^k\right)^2+\left(f_s^k\right)^2-\left(f_s^k-\omega^2\right)^2+\omega^2\left(f_v^k-f_{\Delta v}^k\right)^2}{\left(f_s^k-\omega^2\right)^2+\omega^2\left(f_v^k-f_{\Delta v}^k\right)^2}\right)\\&\approx\sum_{k=1}^{n}\frac{p_kN}{2}\left[\frac{-\omega^4-\omega^2\left(\left(f_{\Delta v}^k\right)^2-2f_s^k-2f_v^kf_{\Delta v}^k\right)}{\left(f_s^k-\omega^2\right)^2+\omega^2\left(f_v^k-f_{\Delta v}^k\right)^2}\right]=\sum_{k=1}^{n}\frac{\omega^2p_kN}{2}\left[\frac{-\omega^2-\left(\left(f_{\Delta v}^k\right)^2-2f_s^k-2f_v^kf_{\Delta v}^k\right)}{\left(f_s^k-\omega^2\right)^2+\omega^2\left(f_v^k-f_{\Delta v}^k\right)^2}\right]\Big\langle 0\end{aligned} \tag{23}$$

Considering that low frequency $\omega\to 0$ gives the strongest constraint on stability, the stability criterion of mixed platoon is obtained as:

$$\sum_{k=1}^{n}p_k\frac{\left(\left(f_{\Delta v}^k\right)^2-2f_s^k-2f_v^kf_{\Delta v}^k\right)}{\left(f_s^k\right)^2}>0 \tag{24}$$

The result is consistent with that in Ward (2009) while it is obtained via the characteristic equation based method. Although Montanino and Punzo (2021) pointed out that, in finite-length platoon, there exists errors for the theoretical results because of the approximation in the deriving process, we adopt the theoretical criterion in the following subsection for the purpose of simplicity.

3.2. Stability of mixed traffic flow

With the general stability criterion of mixed platoon, we examine the stability of mixed platoon of connected vehicles and conventional vehicles in this subsection using the stability region described in Section 2.3. The Taylor expansion coefficients of basic *IDM* after linearisation are:

$$f_s=\frac{2a}{s_e}\left(\frac{s_0+Tv_e}{s_e}\right)^2;f_v=-a\left[\frac{4}{v_0}\left(\frac{v_e}{v_0}\right)^{\delta-1}+\frac{2T(s_0+Tv_e)}{(s_e)^2}\right];f_{\Delta v}=\sqrt{\frac{a}{b}}\frac{v_e}{s_e}\frac{s_0+Tv_e}{s_e} \tag{25}$$

An example is shown in Fig. 3, where three cases of mixed platoon are considered, which are 1) mixed platoon of *LC-IDM* and basic *IDM*, 2) mixed platoon of *HC-IDM* and basic *IDM*, and 3) mixed platoon of *LC-IDM*, *HC-IDM* and basic *IDM*. The setup and model parameters are consistent with those in Fig. 1. In the first two cases, the penetration rates of *CVs* and conventional vehicles are the same, i.e., $p_{(\text{CV-IDM})}=p_{(\text{IDM})}=0.5$, while the penetration rates are $p_{(\text{LC-IDM})}=p_{(\text{HC-IDM})}=0.3$ and $p_{(\text{IDM})}=0.4$ in the third case. The vehicles in the mixed platoon are assumed to be evenly distributed.

From Fig. 3, we can see that the stability of mixed platoon in all three cases are better than that with homogenous *IDM* platoon. More specifically, as shown in Table 2, compared with homogenous *IDM* platoon, the stable region of traffic mixed with *LC-IDM*, *HC-IDM*, and both, increases by 1.75%, 5.19%, and 4.31%, respectively, which indicates that even the partial incorporation of connectivity could improve the string stability of platoon, regardless of driver's compliance level to the received information. However, as compared with Fig. 1, the stability of mixed platoon deteriorates with the incorporation of *IDM*. Particularly, compared with the homogenous *HC-IDM* platoon the stable region of traffic mixed with *LC-IDM*, *HC-IDM*, and both, decreases by 6%, 2.56%, and 3.44%, respectively; and compared with the homogenous *LC-IDM* platoon, the stable region of traffic mixed with *LC-IDM*, *HC-IDM*, and both, decreases by 1.31% and increases by 2.12%, and 1.25%, respectively (which means that the stability of mixed platoons with *HC-IDM* are better than the homogenous *LC-IDM* platoon).

It is also worth noting that in the third case of mixed platoon of all types of vehicles, the platoon jointly benefits from *LC-IDM* and *HC-IDM*. The stability in Fig. 3c increases for the desired time gap under 2.5 s when compared to Fig. 3a (despite being inferior to Fig. 3b) and increases for the desired time gap above 2.5 s when compared to Fig. 3b. This is not surprising because *LC-IDM* tends to

Table 2
Differences (%) in stable regions between mixed traffic and homogenous traffic.

Homogenous Mixed traffic	*IDM*	*LC-IDM*	*HC-IDM*
LC-IDM and *IDM*	1.75%	−1.31%	−6.00%
HC-IDM and *IDM*	5.19%	2.12%	−2.56%
LC-IDM, *HC-IDM* and *IDM*	4.31%	1.25%	−3.44%

dominate the stability at higher desired time gap part and *HC-IDM* tends to dominate the stability at lower desired time gap part. It thus demonstrates that the stability of a platoon is determined and constrained by the stability of vehicles within the platoon which could be inferred from the stability criterion of Eq. (24).

To further investisgate the stability of different platoons in terms of different penetration rates of *CVs* and conventional vehicles, we examine the percentage of unstable area in the stability region for the above-mentioned three cases of mixed platoon. The penetration rate for basic *IDM* (conventional vehicles) ranges from 100% to 0, as the penetration rate of *CVs* increases from 0 to 100%. Regarding the third case, for the sake of simplicity, the penetration rates of *LC-IDM* and *HC-IDM* are always kept as the same.

The results for different platoons' stability are shown in Fig. 4. As we can see in the figure, with the increase of *CVs* (decline of conventional vehicles' proportion), the percentage of unstable area drops from 0.34 to 0.26 (the homogenous *HC-IDM* platoon). The stability of mixed platoon is enhanced as the penetration rate of *CVs* increases, particularly in the case of *HC-IDM*. In addition, as shown by the horizontal dashed line in Fig. 4, incorporating only approximately 20% of *HC-IDM* or 40% of mixed *CVs* (*HC-IDM* and *LC-IDM*) can lead to the same amount of stability improvement as with 100% *LC-IDM*. It further demonstrates that a higher compliance to the received information in the connected environment is more beneficial and critical for stability of the whole platoon.

4. Connected *CF* model with time delay

As one of the most important human factors related to driving behaviour, reaction time has been incorporated in *CF* models since the early stage of traffic flow modelling (Chandler et al., 1958; Saifuzzaman and Zheng, 2014). Although reaction time can be neglected with the introduction of automated vehicle, for connected and/or automated vehicles, time delay can also come from other sources, e.g. delays in sensing, communication, computation, actuation, and etc (Sharma et al., 2019b). More importantly, for human-driven connected vehicles, the reaction time and communication delays jointly influence the *CF* behaviour. Therefore, it is necessary to incorporate the time delay into the *CV* modelling. For the sake of simplicity, here we introduce a constant and identical time delay for all variables in *CV-IDM* to form a time-delayed *CV-IDM* (*TDCV-IDM*), as mathematically defined in Eqs. (26–27). In terms of different compliance levels, incorporating time delay makes *LC-IDM* and *HC-IDM* become time-delayed *LC-IDM* (*TDLC-IDM*) and time-delayed *HC-IDM* (*TDHC-IDM*).

$$a_n(t+\tau) = a\left[1-\left(\frac{v_n}{v_0}\right)^{\delta}-\left(\frac{s^*(v_n,\Delta v_n)}{S_n}\right)^2\right]_t \tag{26}$$

$$s^*(t) = s_0 + (1+U(h_{obv}))Tv_n - \frac{v_n\Delta v_n}{2\sqrt{ab}} \tag{27}$$

The stability criterion for time-delayed *CF* model using the Laplace transform based method is given in (Sun et al., 2018):

$$\frac{1}{2}-\frac{f_{\Delta v}}{f_v}-\frac{f_s}{f_v^2}\geq 0 \,\&\, 1+2\tau(f_v-f_{\Delta v})+\tau^2\left(\frac{1}{2}f_v^2-f_v f_{\Delta v}\right)>0 \tag{28}$$

4.1. Stability analysis of TDCV-IDM

Similar to what is presented in Section 2.3, the string stability regions of *TDCV-IDMs* are drawn for the theoretical result based on Eq. (28) with parameters mentioned before and time delay 0.4 s (which is a typical value for *CVs* (Ngoduy, 2015)), as shown in Fig. 5 (the theoretical stability boundaries of *TD-IDM* and *CV-IDMs* are also plotted for the purpose of comparison). Consistent with *TD-IDM* in Sun et al. (2018), this figure clearly shows the reaction time's negative impact on the stability of *TDCV-IDM*, as the stable region is significantly reduced compared with that of *CV-IDM* in Fig. 1, especially when the maximum acceleration is larger than 1.5 m/s^2, which is probably because of the high-frequency disturbances caused by reaction time (Treiber et al., 2007). It is worth noting that, we

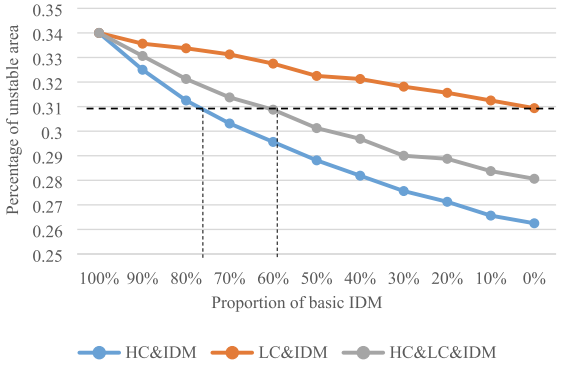

Fig. 4. Comparison of different platoons' stability.

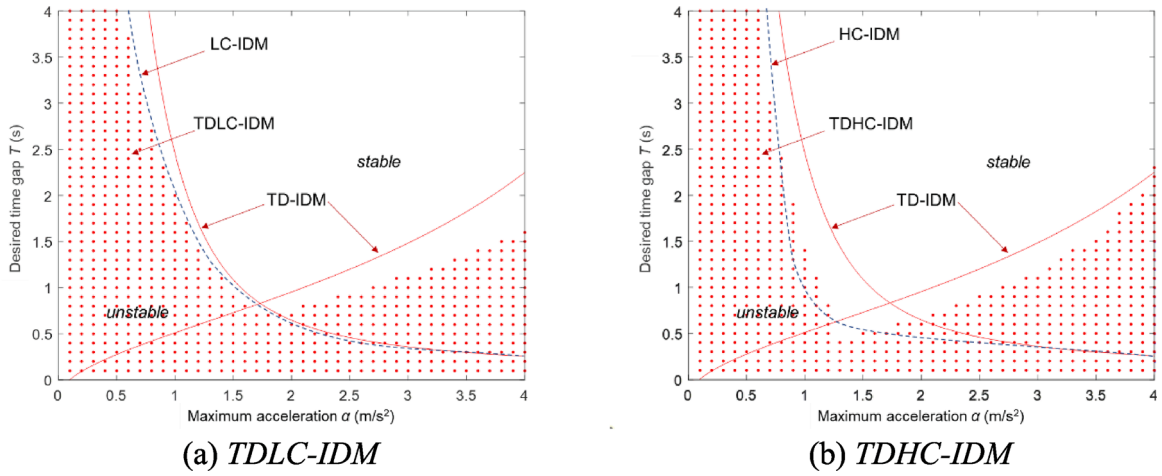

Fig. 5. Theoretical stability regions for *TDCV-IDMs* (the solid line denotes the boundary of the theoretical criterion for *TD-IDM*; the dashed lines denote the approximated boundaries of the theoretical criterion for *CV-IDMs*; the points denote the theoretical string unstable parameter sets for *CV-IDMs*; $\tau = 0.4s$.).

do not consider the impact of vehicle mechanical lag in this study, while as pointed out by Wang (2018) that it further affects the stability distinctly with different disturbance frequencies.

As shown in Fig. 5, although largely attenuated by the time delay, compared with *TD-IDM*, the stability of *TDCV-IDM* is still improved thanks to the incorporation of connectivity. Specifically, when the maximum acceleration is smaller than 1.5 m/s^2, the improvement of stability of *TDLC-IDM* is small, but becomes more significant when the maximum acceleration is more than 1.5 m/s^2; when the maximum acceleration is larger than 1.5 m/s^2, both *TDHC-IDM* and *TDLC-IDM* show significant improvement in stability with a subtle difference: as the maximum acceleration increases, the stability improvement of *TDLC-IDM* tends to increase while the stability improvement of *TDHC-IDM* tends to decline. However, given that human drivers' comfortable maximum acceleration would be smaller than 1.5 m/s^2, the *TDHC-IDM* can benefit more when considering the time delay.

4.2. Comparison between theoretical and simulation results of TDCV-IDMs

As per Sun et al. (2018), the consistency between theoretical and simulation results for TD-*CF* models is easily affected by the time delay. It is also important to compare theoretical and simulation results for *TDCV-IDMs*. Using the same simulation setup as in Section 2.3, we obtain the stability regions of *TDLC-IDM* and *TDHC-IDM* based on simulation results. Fig. 6 is an example of simulation results for *TDCV-IDMs* with the same parameters as in Fig. 5.

Comparing with Fig. 5, we can see that the consistency between theoretical and simulation results is relatively high for the *TDCV-*

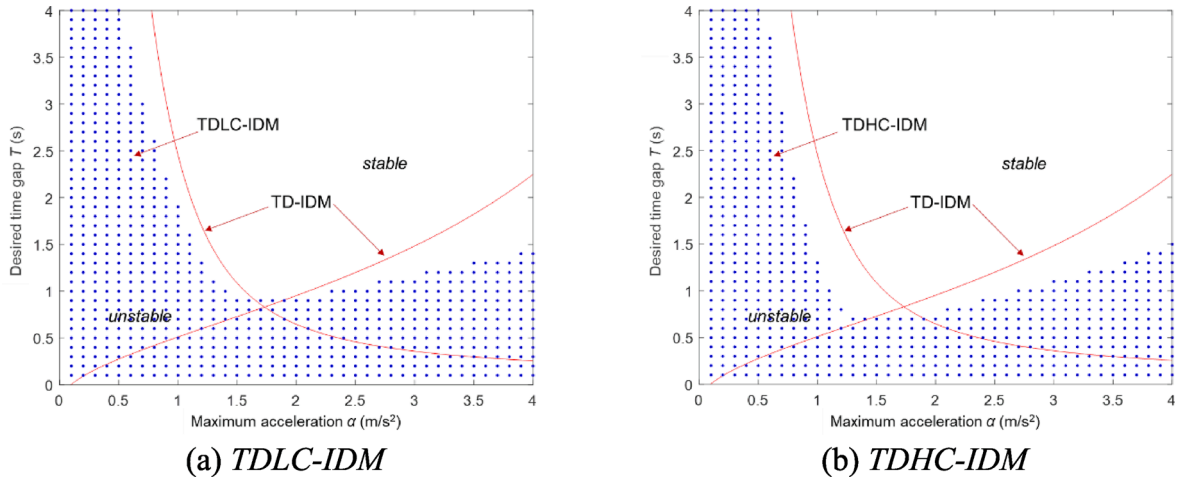

Fig. 6. Stability regions from simulation for *TDCV-IDMs* (The solid line denotes the boundary of the theoretical criterion for *TD-IDM*; the points denote the string unstable parameter sets from simulation for *TDCV-IDMs*; the magnitude of the disturbance in this scenario is 3 m/s: the first vehicle decelerated with 1 m/s^2 for 3 s and then accelerated with 1 m/s^2 for 3 s; $\tau = 0.4s$.).

IDMs when time delay is 0.4 s and the maximum acceleration is larger than 1.5 m/s^2. Once the maximum acceleration exceeds 1.5 m/s^2, the inconsistency between theoretical and simulation results increases. For both *TDCV-IDMs*, the theoretical results seem more conservative than the simulated ones, as more theoretically unstable parameter-sets become stable in simulation results. Again, considering the comfortable acceleration for human drivers, the theoretical results are of practical significance.

Furthermore, since the reaction time is the critical feature of *TDCV-IDMs*, we also investigate the impact of different reaction times on the consistency of simulated and theoretical string stability results with a fixed disturbance. The consistency of theoretical result and simulation result for string stability is evaluated using three indicators (Sun et al., 2018): overall consistency, stability consistency, and instability consistency as defined in Eq. (29). For the confusion matrix in Table 3, *TP* stands for the number of events in which theoretical stable points are identical with simulated stable points, *FN* for the number of events in which simulated stable points are identified as theoretical unstable points, *FP* for the number of events in which simulated unstable point are identified as theoretical stable points, and *TN* for the number of events in which simulated unstable point are identical with theoretical unstable points.

$$Overall\ \ consistency = (TP + TN)/(TP + FP + FN + TN) \tag{29}$$

$$Stablilty\ \ consistency = TP/(TP + FN)$$

$$Instablilty\ \ consistency = TN/(TN + FP)$$

The consistency results are presented in Fig. 7. As shown in this figure, the overall consistency first decreases and then increases with the increase of reaction time, while the stability consistency drops abruptly when the delay exceeds 0.4 s for *TDCV* models. With respect to the instability consistency, it remains at a high level (above 90%). The results indicate that the time delay have a significantly negative affect on the theoretical results, as the theoretical results are much less promising when the time delay is comparatively large (above 0.4 s).

4.3. Impact of time delay on stability

To further quantify the impact of time delay on the *TDCV-IDMs*' stability, we compute the percentage of unstable area within the previously defined stability region to indicate the models' instability. Since a high inconsistency between theoretical and simulation results exists for large time delay as shown in Fig. 7, both the theoretical and simulation results are obtained and compared in this section. With time delay varying from 0.2 s to 1 s, the results of unstable area percentages for both *TDLC-IDM* and *TDHC-IDM* are presented in Fig. 8. More specifically, Fig. 8a illustrates the theoretical results and Fig. 8b illustrates the simulation results with the aforementioned simulation setups. The theoretical and simulation results for *TD-IDM* are presented as well for the sake of comparison.

As we can see from Fig. 8, with the increase of time delay, the percentage of unstable area for both *TDCV-IDM* models steadily increases, both in terms of theoretical and simulation results, while the percentage of unstable area in the theoretical result increases faster than that in the simulation result, which further demonstrates the negative influence of time delay on stability. While compared to *TD-IDM*, the *TDCV-IDM* models are always more stable thanks to the incorporation of connectivity. It is worth noting that the stability for *TDLC-IDM* and *TDHC-IDM* with different time delays changes differently. More specifically, the theoretical results in Fig. 8a reveal that when the time delay is lower than 0.5 s, *TDHC-IDM* is more stable than *TDLC-IDM*, while the difference between *TDLC-IDM* and *TDHC-IDM* becomes negligible when the time delay is higher. A similar trend is observed in the simulation results in Fig. 8b with the acceptance that the threshold of time delay is 0.6 s and the discrepancy between the two models is more obvious. This result is expected since a high compliance to the very delayed information would easily lead to unstable behaviours. This also suggests that with a typical time delay of 0.5 s for connected vehicles, the high compliance to received information is not necessarily beneficial (sometimes even worse) than the low compliance case.

In addition, from the comparison of theoretical and simulation results, it shows that the two models are more unstable in simulations than theoretically expected in the presence of time delay smaller than 0.4 s, whereas they are more stable in simulation results than in theoretical results when the time delay is larger than 0.4 s.

5. Connected *CF* model with estimation errors

While *CV* is commonly assumed to be able to obtain the accurate information of the leading vehicle, human drivers of CVs can still make decision errors that may be attributed to (a) inevitable communication errors in the real world due to faulty devices, communication delay, or loss; (b) drivers making decisions via a combination of received information and own estimation capabilities. Thus, further to the possible time delay for *CV*, we investigate the impact of estimation errors on the stability of traffic flow caused by the *CV*'s imperfect detection and drivers' inaccurate estimation capabilities in this section. Moreover, despite the existence of estimation errors in the connected environment, their amplitudes would be smaller comparing with the conventional environment. We then study

Table 3
Confusion matrix.

	Theoretical stable point	Theoretical unstable point
Simulated stable point	True positive (TP)	False negative (FN)
Simulated unstable point	False positive (FP)	True negative (TN)

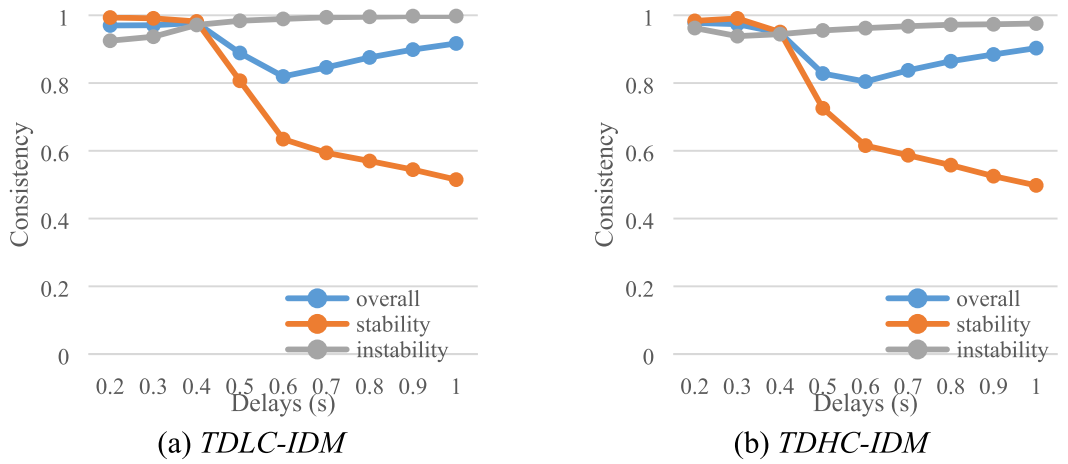

Fig. 7. Consistency results of *CV-IDMs*.

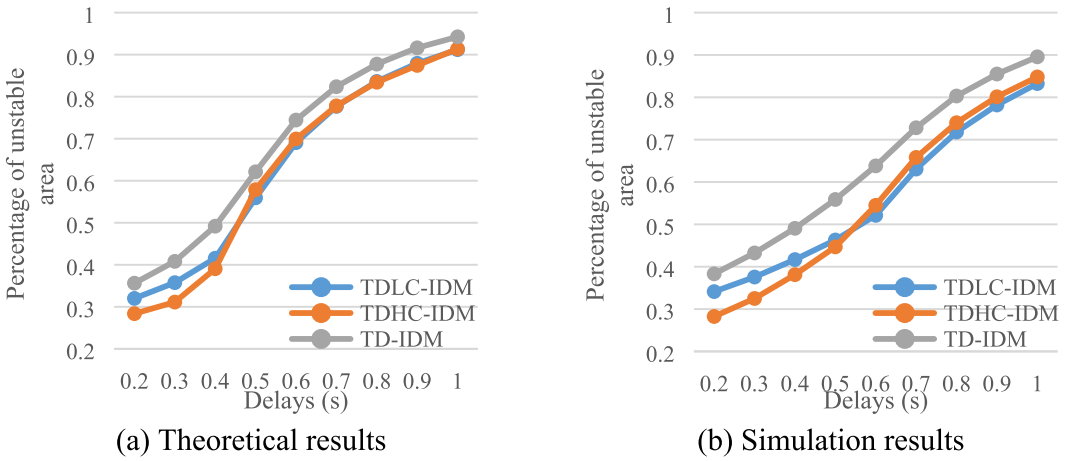

Fig. 8. Stability of *CV-IDMs* with different time delays.

two types of estimation errors by varying the error amplitudes.

In modelling human-driven vehicles, the time-dependent estimation errors for the space gap and the speed difference to the leader are usually incorporated as human factors, as drivers can easily make errors when estimating stimuli. As per Treiber et al. (2006), the estimated space gap s_n^{est} is calculated as shown in Eq. (30):

$$s_n^{est}(t) = s_n(t)e^{V_s w_s(t)} \tag{30}$$

$$w_s(t+\Delta T) = e^{-\Delta t/\tilde{\tau}} w_s(t) + \sqrt{\frac{2\Delta t}{\tau}}\eta(t) \tag{31}$$

where s_n is the actual space gap, V_s is the coefficient of variation and describes the relative standard deviation of s_n^{est} from the true value s_n, and w_s is the Wiener process which describes the temporal evolution of errors in space gap. The estimated relative speed is presented as:

$$\Delta v_n^{est}(t) = \Delta v_n(t) + s_n(t) r_c w_{\Delta v}(t) \tag{32}$$

where r_c is the constant standard deviation of the relative approach rate, and $w_{\Delta V}$ is similar to w_s and describes the temporal evolution of errors in the leader's speed; $\tilde{\tau}$ is the persistence or correlation time. where $\eta(t)$ are independent realisations of a Gaussian distributed quantity with zero mean and variance σ.

We incorporate the same estimation error here for developing the connected *CF* model with estimation errors (EE). *CV-IDM* thus becomes *EECV-IDM* with s_n and v_n replaced by s_n^{est} and Δv_n^{est}, respectively, as shown in Eqs. (33)–(34).

$$a_n(t) = a\left[1 - \left(\frac{v_n}{v_0}\right)^{\delta} - \left(\frac{s^*\left(v_n, \Delta v_n^{est}\right)}{s_n^{est}}\right)^2\right]_t \tag{33}$$

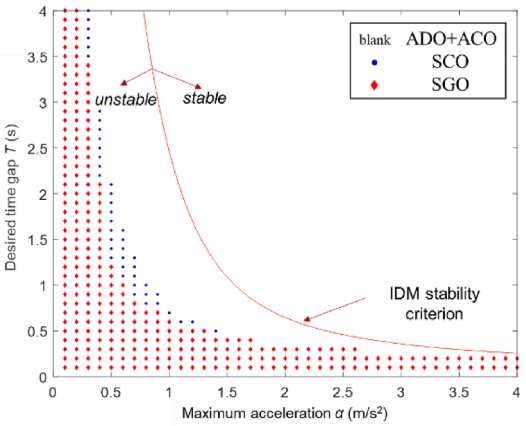

(a) *LC-IDM*

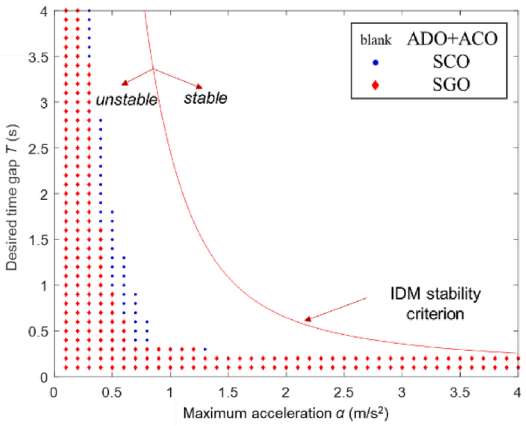

(b) *HC-IDM*

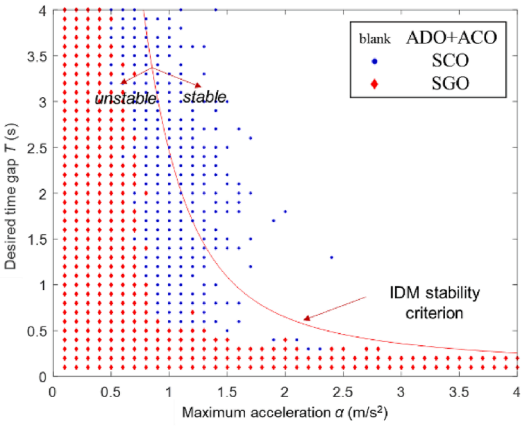

(c) *EELC-IDM*, $\sigma = 0.5$

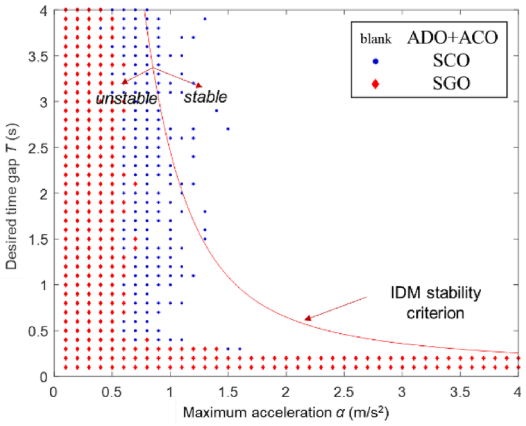

(d) *EEHC-IDM*, $\sigma = 0.5$

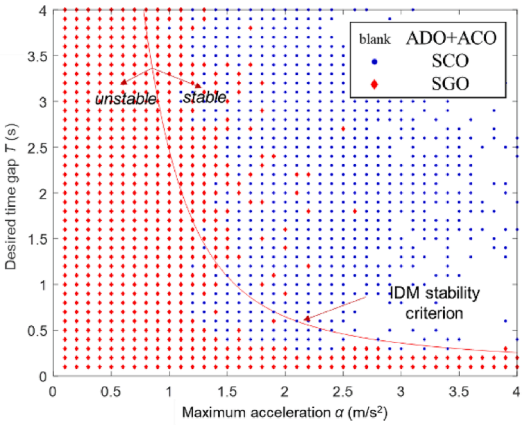

(e) *EELC-IDM*, $\sigma = 1$

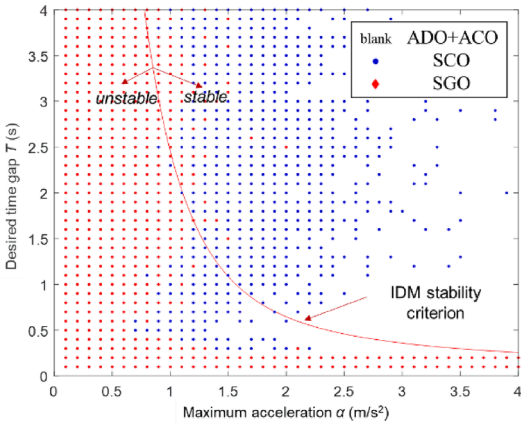

(f) *EEHC-IDM*, $\sigma = 1$,

Fig. 9. Oscillation regions from simulation for *CV-IDMs* and *EECV-IDMs* (The solid curve denotes the boundary between the theoretical stable area and the unstable area for *IDM*; the points denote different types of oscillation from simulation with *EECV-IDMs*; the magnitude of the disturbance in this scenario is 3 m/s: the first vehicle decelerated with 1 m/s^2 for 3 s and then accelerated with 1 m/s^2 for 3 s.).

$$s^*(t) = s_0 + (1 + U(h_{obv}))Tv_n - \frac{v_n \Delta v_n^{est}}{2\sqrt{ab}} \tag{34}$$

5.1. Oscillation analysis of EECV-IDM

Due to the absence of a proper stability criterion with the incorporation of estimation errors for *EECV-IDM*, we can only analyse its stability features with simulation. Furthermore, as the estimation error will lead to all unstable cases in the simulation results according to the conventional stability analysis, we employ the concepts of four types of oscillation proposed in Sun et al. (2020) to analyse the characteristics of different *EECV* models in terms of the resulting congestion severity of traffic flow. These four types of oscillation are defined on the basis of oscillation amplitude (the largest speed drop during the deceleration and acceleration period (Saifuzzaman et al., 2017)) and speed deviation (the difference of lowest speed from initial equilibrium speed), and include amplitude-decay oscillation (*ADO*), amplitude-ceiling oscillation (*ACO*), speed-deviation ceiling oscillation (*SCO*), and speed-deviation growth oscillation (*SCO*). The brief definitions of these oscillations are as follow:

- Amplitude-decay oscillation (*ADO*): The oscillation amplitude strictly decays along the platoon.
- Amplitude-ceiling oscillation (*ACO*): The oscillation amplitudes of following vehicles are not larger than (i.e. ceiled by) the amplitude of the first vehicle.
- Speed-deviation ceiling oscillation (*SCO*): The maximum oscillation amplitude of following vehicles exceeds the amplitude of the first vehicle, but the speed deviations of the following vehicles are constrained by the speed deviation of the first vehicle.
- Speed-deviation growth oscillation (*SGO*): The maximum speed deviation of the following vehicles exceeds the speed deviation of the first vehicle.

The oscillation analysis largely enhance the stability analysis by further distinguishing the unstable region to three oscillation types (*ADO* is similar to the stable region), because traditional stability analysis is on the basis of many unrealistic assumptions (e.g. arbitrarily long platoon, long-wavelength instability, and steady oscillation) (Sun et al., 2020). This enables us to understand the detailed features of oscillation formation and develop more appropriate operational and control strategies tailored to oscillation characteristics and severity.

5.2. Results of oscillation analysis

We run the simulation numerically with the same simulation setup as the previous sections and plot the oscillation regions of *CV-IDMs* and *EECV-IDMs* based on the simulation results. It is worth noting here, similar to stable region, there is extremely rare *ADO* in the simulation results. We thus combine the *ADO* and *ACO* as blank and only plot the *SCO* and *SGO* in the oscillation region as presented in Fig. 9. To study the impact of amplitudes of estimation errors, we also consider two types of estimation errors by varying the variance σ of Gaussian distributed independent function $\eta(t)$ in Eq. (31): $\sigma = 1$ for the typical human-driven vehicles (Treiber et al., 2006), and $\sigma = 0.5$ for smaller estimation errors in the connected environment.

The oscillation regions of *LC-IDM* and *HC-IDM* are first illustrated in Fig. 9a and 9b. Compared with the stability regions of *CV-IDM* shown in Fig. 2, the *SCO* and *SGO* are both in the unstable region and the total area of *SCO* and *SGO* is much smaller than their unstable

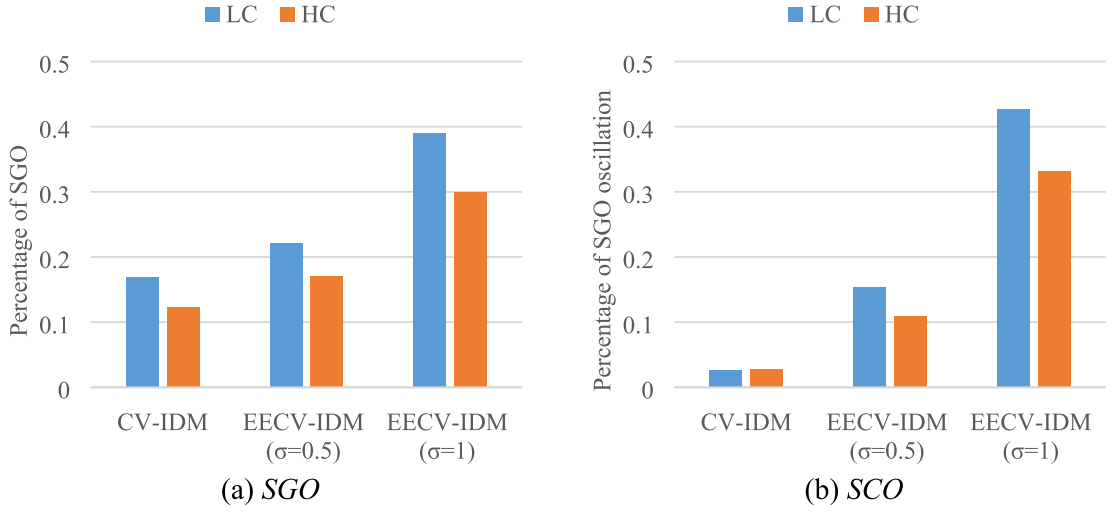

Fig. 10. Comparison of *SGO* and *SCO* regions for *CV-IDMs* and *EECV-IDMs*.

regions (the area of *ACO* is very small although not separately considered here), which is consistent with the oscillation analysis results of *IDM* in Sun et al. (2020). Higher compliance is beneficial for the alleviation of congestion level as less *SGO* area is caused by the *HC-IDM*.

When incorporating estimation errors, as shown in Fig. 9(c-f), more *SCO* and *SGO* forms for the *EECV-IDMs* and the oscillations grow severer as the error amplitudes increase. The oscillation boundaries for all the *EECV-IDMs* are serrated because of the randomness of estimation errors. For both *EELC-IDM* and *EEHC-IDM* with $\sigma = 0.5$, the oscillation areas remain relatively consistent with *LC-IDM* and *HC-IDM* when the desired time gap T is less than 1 s. Once T is greater than 1 s, the *SCO* and *SGO* areas increase rapidly, especially when T is between 1 and 3 s. The same observation can be obtained with larger estimation errors ($\sigma = 1$), while the threshold becomes 0.5 s (i.e., the oscillation areas do not increase substantially if T is less than 0.5 s). Comparing the oscillation areas under different estimation errors, we can see that larger errors lead to much severer congestions, as most of the parameter sets for the *EECV-IDMs* with $\sigma = 1$ will cause the *SCO* or *SGO*, whereas the combined *SCO* and *SGO* area are still close to the unstable region with $\sigma = 0.5$. Overall, the *HC* models outperform the *LC* models in the presence of estimation errors.

To further quantify the impact of estimation errors, we calculate the percentages of *SCO* and *SGO* areas in the oscillation region, respectively, for all the models. While consistent with the conclusions drawn before, the results presented in Fig. 10 also reveal that the increase of *SCO* regions is larger than that of *SGO*: the average increase of *SGO* regions from two *CV-IDMs* to two *EECV-IDMs* ($\sigma = 1$) is 0.2 while the average increase of *SCO* regions is 0.35. This suggests that the estimation errors are more related to the congestion with less severity and, in turn demonstrates the necessity of classifying oscillation into these four types as well.

6. Conclusions

This paper aims to investigate the stability characteristics of a newly proposed *CF* model for human-driven *CVs* which considers the driver compliance factor using the Prospect Theory. Specifically, two levels of driver compliance, i.e., low compliance and high compliance, were defined and incorporated into *IDM*. Based on the general stability criterion for *CF* model without considering any time delays, we analysed and compared the theoretical and simulated stability results for *CV-IDMs*. The results indicate that the *CF* stability is improved with the connected environment, while a higher compliance to the information leads to a higher enhancement of the stability.

In addition, considering the two compliance levels of *CVs* and mixed traffic flow with conventional human-driven vehicles, we studied the stability of heterogenous traffic by deriving the criterion with Laplace transform based method. By comparing the stability of different platoon setups in terms of different penetration rates of *CVs* and conventional vehicles, we further demonstrated that a higher penetration of high-compliance *CVs* in the connected environment is more beneficial for the whole platoon's stability.

Moreover, regardless of the driver compliance to the information, we extended *CV-IDM* by considering two important additional human factors, i.e., time delay and estimation error, and investigated the new models' stability and oscillation features. We first evaluated the stability of *CV-IDM* models with time delays for high compliance drivers and low compliance drivers, respectively, and found that the time delay in *CV* significantly deteriorate the *CF* stability even in the connected environment. Our simulation results imply that the time delay also affects the consistency of theoretical and simulated results. Compared with the models for low compliance drivers, with the increase of time delay, the *CV-IDM* model for high-compliance drivers will become more unstable, and the inconsistency between the theoretical and simulated results become larger.

Finally, we incorporated the time-dependent estimation errors of space gap and speed difference elements into the *CV-IDM* model and analysed the models' oscillation characteristics resulted from the estimation errors. We found that the estimation errors cause more oscillations; and that as the error amplitude increases the oscillations become more severe. However, drivers' higher compliance to the information can still alleviate the congestion severity.

Given that only human driven CVs were considered and the driver compliances are identical within the same group of drivers in this study, potential future directions could be considering the intra-driver compliance heterogeneity in the modelling framework and analysing the stability of mixed traffic flow of CVs, automated vehicles and human-driven only vehicles with different platoon spatial distributions.

CRediT authorship contribution statement

Jie Sun: Conceptualization, Data curation, Formal analysis, Investigation, Methodology, Software, Validation, Writing – original draft. **Zuduo Zheng:** Conceptualization, Formal analysis, Funding acquisition, Investigation, Methodology, Supervision, Validation, Writing – review & editing. **Anshuman Sharma:** Formal analysis, Investigation, Validation, Writing – review & editing. **Jian Sun:** Formal analysis, Investigation, Validation, Writing – review & editing.

Declaration of Competing Interest

The authors declare that they have no known competing financial interests or personal relationships that could have appeared to influence the work reported in this paper.

Acknowledgements

This research was partially funded by the Australian Research Council (ARC) (DP210102970). Jian Sun's involvement was partially

funded by NSFC (The national science foundation of China) 52125208 and 52232015. The authors are grateful for the insightful comments from anonymous reviewers.

References

Bando, M., Hasebe, K., Nakanishi, K., Nakayama, A., 1998. Analysis of optimal velocity model with explicit delay. Phys. Rev. E 58, 5429.
Chandler, R.E., Herman, R., Montroll, E.W., 1958. Traffic dynamics: studies in car following. Oper. Res. 6, 165–184.
Diakaki, C., Papageorgiou, M., Papamichail, I., Nikolos, I., 2015. Overview and analysis of vehicle automation and communication systems from a motorway traffic management perspective. Transp. Res. A Policy Pract. 75, 147–165.
Ge, J.I., Orosz, G., 2014. Dynamics of connected vehicle systems with delayed acceleration feedback. Transportation Research Part C: Emerging Technologies 46, 46–64.
Hamdar, S.H., Treiber, M., Mahmassani, H.S., Kesting, A., 2008. Modeling driver behavior as sequential risk-taking task. Transp. Res. Rec. 2088, 208–217.
Hamdar, S.H., Dixit, V.V., Talebpour, A., Treiber, M., 2020. A behavioral microeconomic foundation for car-following models. Transportation research part C: emerging technologies 113, 228–244.
Herman, R., Montroll, E.W., Potts, R.B., Rothery, R.W., 1959. Traffic dynamics: analysis of stability in car following. Oper. Res. 7, 86–106.
Jia, D., Ngoduy, D., 2016. Enhanced cooperative car-following traffic model with the combination of V2V and V2I communication. Transp. Res. B Methodol. 90, 172–191.
Jia, D., Ngoduy, D., Vu, H., 2019. A multiclass microscopic model for heterogeneous platoon with vehicle-to-vehicle communication. Transportmetrica B: Transport Dynamics 7, 448–472.
Jia, D., Sun, J., Sharma, A., Zheng, Z., Liu, B., 2021. Integrated simulation platform for conventional, connected and automated driving: A design from cyber–physical systems perspective. Transportation Research Part C: Emerging Technologies 124, 102984.
Kahneman, D., Tversky, A., 2013. Prospect theory: An analysis of decision under risk. Part I. World Scientific, Handbook of the fundamentals of financial decision making, pp. 99–127.
Milanés, V., Shladover, S.E., 2014. Modeling cooperative and autonomous adaptive cruise control dynamic responses using experimental data. Transportation Research Part C: Emerging Technologies 48, 285–300.
Montanino, M., Punzo, V., 2021. On string stability of a mixed and heterogeneous traffic flow: A unifying modelling framework. Transp. Res. B Methodol. 144, 133–154.
Monteil, J., Billot, R., Sau, J., El Faouzi, N.-E., 2014. Linear and weakly nonlinear stability analyses of cooperative car-following models. IEEE Trans. Intell. Transp. Syst. 15, 2001–2013.
Ngoduy, D., 2013. Analytical studies on the instabilities of heterogeneous intelligent traffic flow. Commun. Nonlinear Sci. Numer. Simul. 18, 2699–2706.
Ngoduy, D., 2015. Linear stability of a generalized multi-anticipative car following model with time delays. Commun. Nonlinear Sci. Numer. Simul. 22, 420–426.
Orosz, G., Wilson, R.E., Szalai, R., Stépán, G., 2009. Exciting traffic jams: nonlinear phenomena behind traffic jam formation on highways. Phys. Rev. E 80, 046205.
Orosz, G., Wilson, R.E., Stépán, G., 2010. Traffic jams: dynamics and control. Philos. Trans. R. Soc. A Math. Phys. Eng. Sci. 368, 4455–4479.
Orosz, G., Moehlis, J., Bullo, F., 2011. Delayed car-following dynamics for human and robotic drivers, *ASME 2011 International Design Engineering Technical Conferences and Computers and Information in Engineering Conference*. Am. Soc. Mech. Eng. 529–538.
Rahman, M.H., Abdel-Aty, M., Wu, Y., 2021. A multi-vehicle communication system to assess the safety and mobility of connected and automated vehicles. Transportation research part C: emerging technologies 124, 102887.
Saifuzzaman, M., Zheng, Z., 2014. Incorporating human-factors in car-following models: a review of recent developments and research needs. Transportation Research Part C: Emerging Technologies 48, 379–403.
Saifuzzaman, M., Zheng, Z., Haque, M.M., Washington, S., 2017. Understanding the mechanism of traffic hysteresis and traffic oscillations through the change in task difficulty level. Transp. Res. B Methodol. 105, 523–538.
Sau, J., Monteil, J., Billot, R., El Faouzi, N.-E., 2014. The root locus method: application to linear stability analysis and design of cooperative car-following models. Transportmetrica B: Transport Dynamics 2, 60–82.
Sau, J., Monteil, J., Bouroche, M., 2019. State-space linear stability analysis of platoons of cooperative vehicles. Transportmetrica B: Transport Dynamics 7, 18–43.
Sharma, A., Ali, Y., Saifuzzaman, M., Zheng, Z., Haque, M.M., 2017. Human Factors in Modelling Mixed Traffic of Traditional, Connected, and Automated Vehicles. *International Conference on Applied Human Factors and Ergonomics*. Springer 262–273.
Sharma, A., Zheng, Z., Bhaskar, A., Haque, M.M., 2019a. Modelling car-following behaviour of connected vehicles with a focus on driver compliance. Transp. Res. B Methodol. 126, 256–279.
Sharma, A., Zheng, Z., Kim, J., Bhaskar, A., Haque, M.M., 2019b. Estimating and comparing response times in traditional and connected environments. Transp. Res. Rec. 2673, 674–684.
Sharma, A., Zheng, Z., Kim, J., Bhaskar, A., Haque, M.M., 2021. Assessing traffic disturbance, efficiency, and safety of the mixed traffic flow of connected vehicles and traditional vehicles by considering human factors. Transportation research part C: emerging technologies 124, 102934.
Sun, J., Sun, J., 2018. Investigating the oscillation characteristics and mitigating its impact with low-penetration connected and automated vehicles. In: *2018 21st International Conference on Intelligent Transportation Systems (ITSC)*. IEEE, pp. 2339–2345.
Sun, J., Zheng, Z., Sun, J., 2018. Stability analysis methods and their applicability to car-following models in conventional and connected environments. Transp. Res. B Methodol. 109, 212–237.
Sun, J., Zheng, Z., Sun, J., 2020. The relationship between car following string instability and traffic oscillations in finite-sized platoons and its use in easing congestion via connected and automated vehicles with IDM based controller. Transp. Res. B Methodol. 142, 58–83.
Sun, J., Zheng, Z., Sun, J., 2023. Stability evolution of car-following models considering asymmetric driving behaviour. Transp. Res. Rec. 03611981231156584.
Swaroop, D., Hedrick, J., 1996. String stability of interconnected systems. IEEE Trans. Autom. Control 41, 349–357.
Talebpour, A., Mahmassani, H.S., 2016. Influence of connected and autonomous vehicles on traffic flow stability and throughput. Transportation Research Part C: Emerging Technologies 71, 143–163.
Talebpour, A., Mahmassani, H.S., Hamdar, S.H., 2011. Multiregime sequential risk-taking model of car-following behavior: specification, calibration, and sensitivity analysis. Transp. Res. Rec. 2260, 60–66.
Talebpour, A., Mahmassani, H.S., Bustamante, F.E., 2016. Modeling driver behavior in a connected environment: Integrated microscopic simulation of traffic and mobile wireless telecommunication systems. Transp. Res. Rec. 2560, 75–86.
Treiber, M., Kanagaraj, V., 2015. Comparing numerical integration schemes for time-continuous car-following models. Physica A 419, 183–195.
Treiber, M., Kesting, A., Helbing, D., 2006. Delays, inaccuracies and anticipation in microscopic traffic models. Physica A 360, 71–88.
Treiber, M., Kesting, A., Helbing, D., 2007. Influence of reaction times and anticipation on stability of vehicular traffic flow. Transportation Research Record: Journal of the Transportation Research Board 23–29.
Treiber, M., Kesting, A., 2013. Traffic flow dynamics: Data. Springer-Verlag, Berlin Heidelberg, Models and Simulation.
Treiber, M., Hennecke, A., Helbing, D., 2000. Congested traffic states in empirical observations and microscopic simulations. Phys. Rev. E 62, 1805.
van Arem, B., van Driel, C.J., Visser, R., 2006. The impact of cooperative adaptive cruise control on traffic-flow characteristics. IEEE Trans. Intell. Transp. Syst. 7, 429–436.
van Lint, J., Calvert, S.C., 2018. A generic multi-level framework for microscopic traffic simulation—Theory and an example case in modelling driver distraction. Transp. Res. B Methodol. 117, 63–86.
Wang, M., 2018. Infrastructure assisted adaptive driving to stabilise heterogeneous vehicle strings. Transportation Research Part C: Emerging Technologies 91, 276–295.

Ward, J.A., 2009. Heterogeneity, lane-changing and instability in traffic: A mathematical approach. University of Bristol.
Wilson, R.E., 2008. Mechanisms for spatio-temporal pattern formation in highway traffic models. Philos. Trans. R. Soc. A Math. Phys. Eng. Sci. 366, 2017–2032.
Wilson, R.E., Ward, J.A., 2011. Car-following models: fifty years of linear stability analysis–a mathematical perspective. Transp. Plan. Technol. 34, 3–18.
Xie, D.-F., Zhao, X.-M., He, Z., 2018. Heterogeneous traffic mixing regular and connected vehicles: Modeling and stabilization. IEEE Trans. Intell. Transp. Syst. 20, 2060–2071.
Zhang, X., Jarrett, D.F., 1997. Stability analysis of the classical car-following model. Transp. Res. B Methodol. 31, 441–462.
Zhang, L., Orosz, G., 2016. Motif-based design for connected vehicle systems in presence of heterogeneous connectivity structures and time delays. IEEE Trans. Intell. Transp. Syst. 17, 1638–1651.
Zhou, Y., Ahn, S., Wang, M., Hoogendoorn, S., 2020. Stabilizing mixed vehicular platoons with connected automated vehicles: An H-infinity approach. Transp. Res. B Methodol. 132, 152–170.